

Contract No.:

This manuscript has been authored by Savannah River Nuclear Solutions (SRNS), LLC under Contract No. DE-AC09-08SR22470 with the U.S. Department of Energy (DOE) Office of Environmental Management (EM).

Disclaimer:

The United States Government retains and the publisher, by accepting this article for publication, acknowledges that the United States Government retains a non-exclusive, paid-up, irrevocable, worldwide license to publish or reproduce the published form of this work, or allow others to do so, for United States Government purposes.

PVT-15-1195 (for ASME Journal of Pressure Vessel Technology Special Issue: 50th Anniversary of the ASME Pressure Vessels and Piping Division)

Title:

Flaw Stability Considering Residual Stress for Aging Management of Spent Nuclear Fuel Multiple-Purpose Canisters

Authors:

(1) Poh-Sang Lam

Materials Science and Technology
Savannah River National Laboratory
Aiken, SC 29808, USA
ps.lam@srnl.doe.gov

(2) Robert L. Sindelar

Materials Science and Technology
Savannah River National Laboratory
Aiken, SC 29808, USA
robert.sindelar@srnl.doe.gov

ABSTRACT

A typical multipurpose canister (MPC) is made of austenitic stainless steel and is loaded with spent nuclear fuel assemblies. Because heat treatment for stress relief is not required for the construction of the MPC, the canister is susceptible to stress corrosion cracking in the weld or heat affected zone regions under long-term storage conditions. Logic for flaw acceptance is developed should crack-like flaws be detected by Inservice Inspection. The procedure recommended by API 579-1/ASME FFS-1, Fitness-for-Service, is used to calculate the instability crack length or depth by failure assessment diagram. It is demonstrated that the welding residual stress has a strong influence on the results.

INTRODUCTION

One of the options to close the nuclear fuel cycle is to dispose of the spent nuclear fuel (SNF) in a permanent geological repository. However, before the repository is identified and approved for use, the continued safe storage until final disposition of SNF is a challenge to the nuclear industry. The SNF are initially placed in

storage pools (wet storage) for sufficient time to allow cooling via radioactive decay and then transferred to dry cask storage facilities. The present licensing basis for dry cask storage is up to 60 years (20-year initial license and 40-year re-license) but longer storage times may become necessary as the U.S. Department of Energy (DOE) and the U. S. Nuclear Regulatory Commission (NRC) evaluate repository options in a once-through strategy, and/or reprocessing options under modified open cycle or full recycle strategies. In clarification of the regulatory basis for continued storage, the NRC has recently established the rule for Continued Storage of Spent Nuclear Fuel [1] that will allow, in principle, re-licensing of storage systems for many additional decades.

Many Independent Spent Fuel Storage Installations (ISFSIs) are located near the coastal regions. Because the stainless steel canisters in these dry storage systems were not stress relieved for the welding residual stress, chloride induced stress corrosion cracking (CISCC) might take place under temperature and humidity conditions with marine salt and other atmospheric deposit contaminants [2-12]. When this crack grows to approach the instability crack size, it will compromise the safety-credited containment boundary of the storage system such as the multipurpose canisters (MPC).

Non-destructive evaluation (NDE) or non-destructive testing (NDT) techniques are being developed to deploy sensors through the narrow annular space in the dry cask system to detect service-induced planar and non-planar flaws (e.g., cracking and pitting) on the surface of the canister. Flaw acceptance criteria are needed for the disposition of the inspection results should relevant indications be found. Recently, instability crack lengths and depths were reported for through-wall and part-through-wall cracks in these canisters [13]. The analysis was based on ASME Boiler and Pressure Vessel Code Section XI [14] with a limit load approach which depends on the material's minimum tensile properties as provided by the ASME Section II [15]. The welding residual stress was not considered.

In a previous paper [16], the development of a fracture mechanics-based flaw evaluation protocol to establish flaw stability criteria for these canisters was outlined, based on the API 579-1/ASME FFS-1 codified procedure for Fitness-for-Service [17] with the failure assessment diagram (FAD) methodology. That protocol is applied in the current analysis. The welding residual stresses for the longitudinal or axial (seam) weld and for the circumferential (girth) weld, respectively, are estimated based on API 579 recommendation since the welding parameters are proprietary information and hence are not available for this analysis. For a direct comparison of the flaw tolerance results, the loading conditions, tensile properties (Type 304 stainless steel), and the (bounding) flaw configurations are selected identically to those in Reference [13]. The geometry of the Holtec HI-STORM canister [18,19] is used for the current work. Because the FAD is used in the development of flaw stability criteria, the fracture toughness (K_{IC}) of the material is needed and is obtained through API 579 recommendation with a reference to the material test data obtained previously [20].

It was found that when the residual stress is included as part of the loading, and with the consideration of elastic-plastic fracture mechanics through the FAD formulation, the resulting instability crack sizes have been

significantly reduced from those based on the net section yielding limit load approach [13]. The results are reported in this paper.

CONSTRUCTION AND LOADING OF MPC

Various canister designs have been used to store fuel at ISFSIs. In the present work, a typical cask system, Holtec International Storage Module, (HI-STORM) [18,19] is selected for the calculation of instability crack sizes in the development of acceptance criteria for structural integrity assessment. This MPC is a cylindrical shell with all components made of austenitic stainless steel (Typically, 304 stainless steel) [18]. The height of the canister is 4.8 m (15.8 ft) with an outer diameter 1.73 m (5.7 ft) and the thickness of the shell is 1.27 cm (0.5 in.).

The cylindrical shell is constructed with a circumferential (girth) weld in the mid-height and four axial seam welds (Fig. 1). The upper and lower axial welds are offset slightly along the circumferential weld. The shell is welded to a bottom plate with a thickness of 6.35 cm (2.5 in.) [18]. Submerged arc welding (SAW) with full penetration is applied. Although the post-weld nondestructive inspection is carried out, the heat treatment to relieve the welding residual stress is not required for the construction. The flaw stability criteria will be developed for postulated cracks in the heat affected zone (HAZ) in these critical locations.

The fuel assemblies are loaded vertically into HI-STORM canister. The total weight of the loaded canister is about 36 metric tons or 40 tons (see Table 1). The closure welds in the lid region were not considered in the MPC failure assessment [1] because 1) the tungsten inert gas (TIG) welds in the lid region are tougher than the submerged arc welds in the canister shell and the baseplate; 2) the multiple layers of welds (between the closure ring and shell; and between the lid and shell) provide redundant safety features for the lid, and 3) the lower stresses are expected in the lid. Therefore, flaw stability criteria are not developed for closure welds.

The loading conditions that are used to evaluate flaw stability by calculating the instability crack sizes are listed in Table 1. Both normal and accident conditions are included, and are identical to those employed in a previous flaw tolerance analysis [13] based on limit load [14].

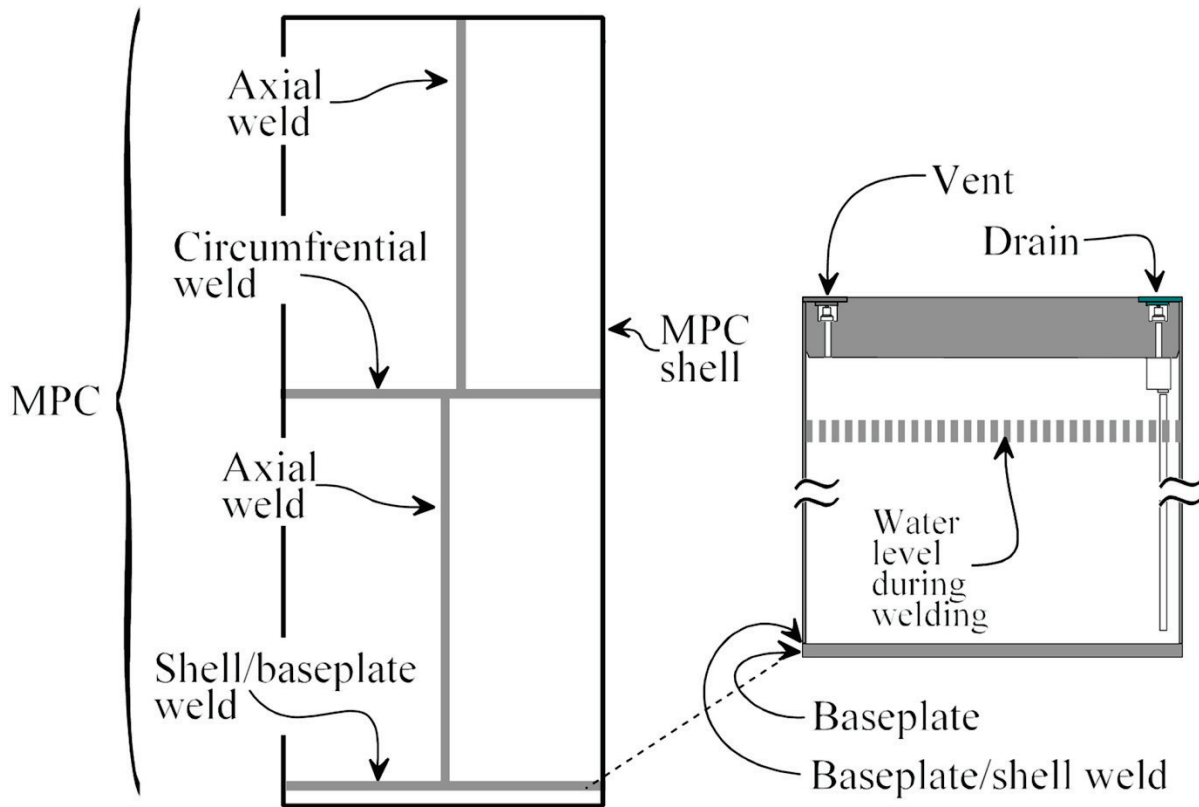


Figure 1 Welds on a Multipurpose Canister (Reproduced from NUREG-1864 [18], Fig. 16)

Table 1 Load Cases for Canister HI-STORM [13]

Loading Case	Design Internal Pressure MPa (psig)	Loaded Canister Mass kg (kips)	Axial Handling Load or Acceleration
Normal	0.69 (100)	40800 (90)	1.15g
Accident	1.38 (200)	40800 (90)	1.15g

FRACTURE METHODOLOGY

The initiation and growth of stress corrosion cracks, in particular, CISCC, as postulated on the external surface of an austenitic stainless steel canister in the HAZ is elastic-plastic in nature. The welding residual stress is expected to play an important role in the subcritical crack growth until the instability length (for a through-wall flaw) or depth (for a part-through-wall flaw) is reached. To include all the contributory factors in the

development of flaw disposition technology, it appears that API 579-1/ASME FFS-1, Fitness-For-Service code [17] is an appropriate choice. It is emphasized that *citation of this code does not imply that it is the adopted code of record for flaw disposition for the canisters at ISFSIs.*

API 579 recommends that Level 3 Assessment be used if subcritical crack growth is possible while the structural component is in service. The Level 3 Method A Assessment requires that the use of the Level 2 Assessment procedure and the FAD with *user specified* Partial Safety Factors based on risk assessments, which are unavailable for the current analysis. It was then decided that the Level 2 Assessment be conducted to establish the flaw stability criteria, and to defer the extra requirements to meet the Level 3 Assessment (e.g., *user specified* Partial Safety Factors) for future work, or to properly adjust the inspection results when the indication is found by inservice inspection. This deviation from the code allows a direct comparison of the results between the API 579 FAD approach and the limit load approach used in Reference [13], where the safety factors were not applied.

The main components of API 579 approach are the determination of the welding residual stress and the formulation of the failure assessment diagram. These are discussed in the following sections.

Welding Residual Stress

Four flaw configurations (Figs. 2 to 5) in the HAZ are considered: Case 1) Axial crack parallel to an axial (or longitudinal) weld with dominant residual stress perpendicular to the weld (to open the crack), Case 2) Axial crack perpendicular to a circumferential (girth) weld with dominant residual stress parallel to the weld, Case 3) Circumferential crack parallel to a circumferential weld with dominant residual stress perpendicular to the weld, and Case 4) Circumferential crack perpendicular to an axial weld with dominant residual stress parallel to the weld. The respective residual stresses can be estimated by API 579 procedures if the actual measurement or numerical simulation is not available. The major inputs for the calculations recommended in API 579 Annex E *Residual Stress in a Fitness-for-Service Evaluation* [17] include the following:

1. Yield Stress – If no actual yield strength is available, then the yield stress used to estimate the residual stress is $\sigma_{ys}^r = \sigma_{ys} + 69 \text{ MPa}$ (or $\sigma_{ys}^r = \sigma_{ys} + 10 \text{ ksi}$), where σ_{ys}^r is the magnitude of the effective yield strength used to estimate the residual stress, and σ_{ys} is the specified minimum yield strength of the material. The 69 MPa (10 ksi) elevation from the minimum yield strength is to account for the actual material properties, which are typically higher than the code minimum requirements. From ASME Boiler and Pressure Vessel Code, Section II, Part D, [15], the minimum yield strength listed in its Table 1A for 304 stainless steel is 205 MPa (30 ksi) and the minimum tensile strength (UTS) is 515 MPa (75 ksi). Note that for the current analysis with API 579 Level 2 (or Level 3) Assessment [17], the flow stress, and thus the

UTS, is not used. Also note that the maximum temperature limit for using these properties is 427 °C (800 °F) for ASME Section III Classes 2 and 3 pressure vessels.

2. Welding Parameters – API 579 Annex E [17] provides estimation equations for calculating the membrane and bending components of the residual stress. The key input parameter is the heat input density (\hat{Q}), which is a function of linear heat input to the weld $\dot{q} = (IV\eta)/u$, where I is the welding electric current, V is the welding voltage, and η is welding arc efficiency, and u is the welding travel speed. However, these parameters are proprietary information and are not for public dissemination. Therefore, from API 579 Annex E, Table E.1M [17], a suggested value of 1080 J/mm is selected as the average heat input in the analysis. This average heat input was based on a 4 mm electrode, 889 mm/min travel speed, with 500A-32V for stainless steel with submerged arc welding. The code [17] also provides the upper bound heat input of 1920 J/mm, which was based on 750A-38V but is not used in the current work.

Once the heat input density parameter \hat{Q} is determined, the API 579 Annex E Sections E.4.2 (double V-groove circumferential welds) and E.4.4 (double V-groove longitudinal welds) [17] provide estimation equations for the residual stress parameters $\bar{\sigma}_m^r$, $\bar{\sigma}_b^r$, s_0^r , and s_i^r , where $\bar{\sigma}_m^r$ and $\bar{\sigma}_b^r$ are, respectively, the normalized membrane and bending components of the residual stress, $s_0^r = K - |\bar{\sigma}_m^r| - |\bar{\sigma}_b^r|$, $s_i^r = 0.25s_0^r$, and $K=1.2$ or 1.5 depending on whether the residual stress is perpendicular or parallel to the weld, respectively. These parameters are polynomial functions of \hat{Q} and \hat{R} ($\hat{R} = r/t$, where r is the vessel mean radius and t is the nominal vessel thickness; but $\hat{R} = 30$ when $r/t < 30$). The equations for $\bar{\sigma}_m^r$ and $\bar{\sigma}_b^r$ are too cumbersome to be listed in this paper. A position-dependent normalized residual stress factor D is then given as $D = \bar{\sigma}_m^r + \bar{\sigma}_b^r(2\zeta - 1) + A - B$, where $A = \left(\frac{s_0^r - s_i^r}{2}\right)(2\zeta - 1)^3$, $B = (s_0^r + s_i^r) \left\{ \frac{[\sin(\pi(2\zeta - 1) + C)]}{2\sin(C)} \right\}$, $C = \arctan \left[\frac{5}{\pi} \left(\frac{s_0^r + s_i^r}{s_0^r - s_i^r} \right) \right]$, and $\zeta = \frac{x}{t}$ (see Eqs. E.8 to E.12 in API 579 Annex E [17]). It should be noted that, in these equations, x is measured from the inner surface of the vessel wall. The direction of x will be reversed (denoted as x' as shown in Table 2) when an external surface crack is considered ($x'=0$ at the external surface of the cylinder). The first two terms in the expression for D are the membrane and bending components, respectively, and the last two terms (A and B) represent the self-equilibrating component. According to API 579 Annex E, Eqs. E.6, E.7, E.13, and E.14 [17], the value of D must be limited not to exceed K in tension or $-K$ in compression. This adjusted parameter of D is denoted as parameter \hat{E} , and the residual stress (σ^r) across the thickness of the vessel wall is given by API 579 Annex E, Eq. E.5 [17] as

$$\sigma^r(\zeta) = \hat{E} \sigma_{ys}^r R_r \quad (1)$$

where R_r is the reduction in residual stress related to the test pressure. In the present analysis R_r is taken as 1.0 (no reduction).

The estimated residual stresses through the thickness of the canister wall for the four flaw configurations, calculated from Eq. (1), are shown in Figures 2 to 5. These figures also show the variations of the linear and the self-equilibrating parts of the residual stress through the thickness of the canister wall. Each of the residual stress (RS) distribution is fitted with a fourth order polynomial (Table 2), and its coefficients (σ_0 , σ_1 , σ_2 , σ_3 , and σ_4) can be used to calculate the stress intensity factor based on API 579 Annex C *Compendium of Stress Intensity Factor Solutions* [17]. These coefficients may also be used for calculating the reference stress (API 579 Annex D *Compendium of Reference Stress Solutions for Crack-like Flaws*, [17]), but instead the membrane and bending parts of the residual stress are often used (see Eqs. (11) and (12) in a later section) because of convenience as how the equations are written. Note that in Table 2 the coordinate x' in the fourth-order polynomial is reversed with respect to Figures 2 to 5 due to the sign convention for flaws located on the outside surface of the canister (present case).

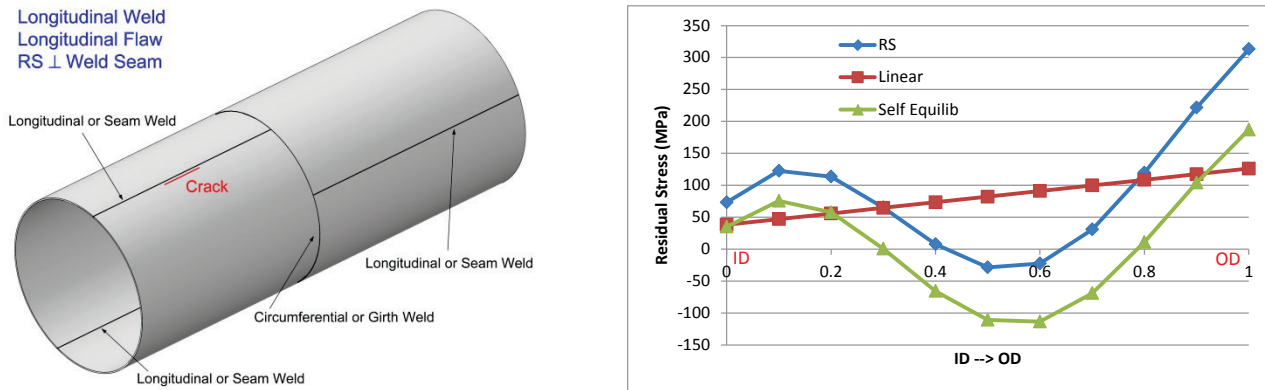


Figure 2 Case 1: Axial Crack Parallel to an Axial Weld - Residual Stress (RS) Perpendicular to the Axial Weld with a Double-V Notch

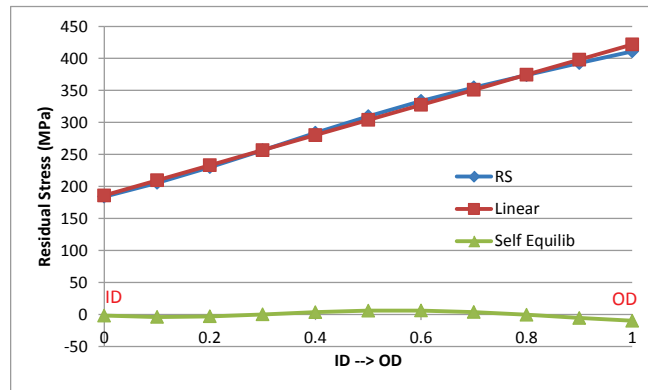
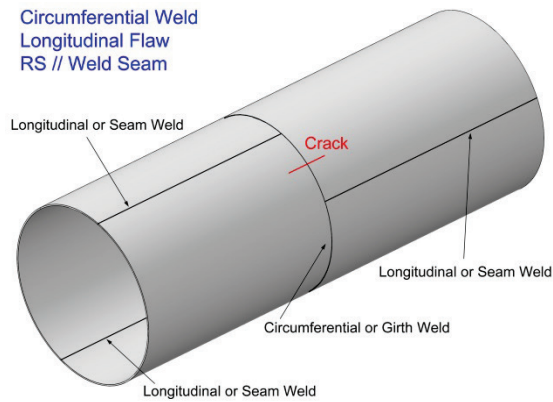


Figure 3 Case 2: Axial Crack Perpendicular to a Circumferential Weld - Residual Stress Parallel to the Circumferential Weld with a Double-V Notch

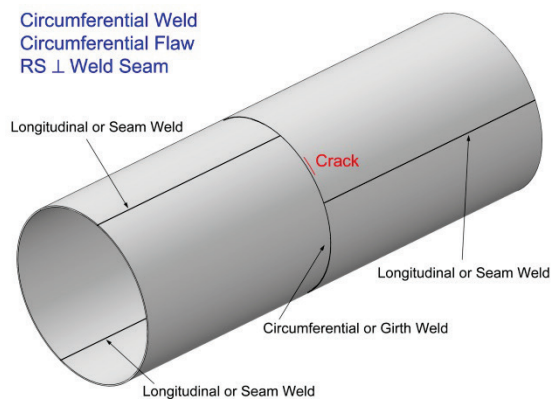


Figure 4 Case 3: Circumferential Crack Parallel to a Circumferential Weld - Residual Stress Perpendicular to the Circumferential Weld with a Double-V Notch

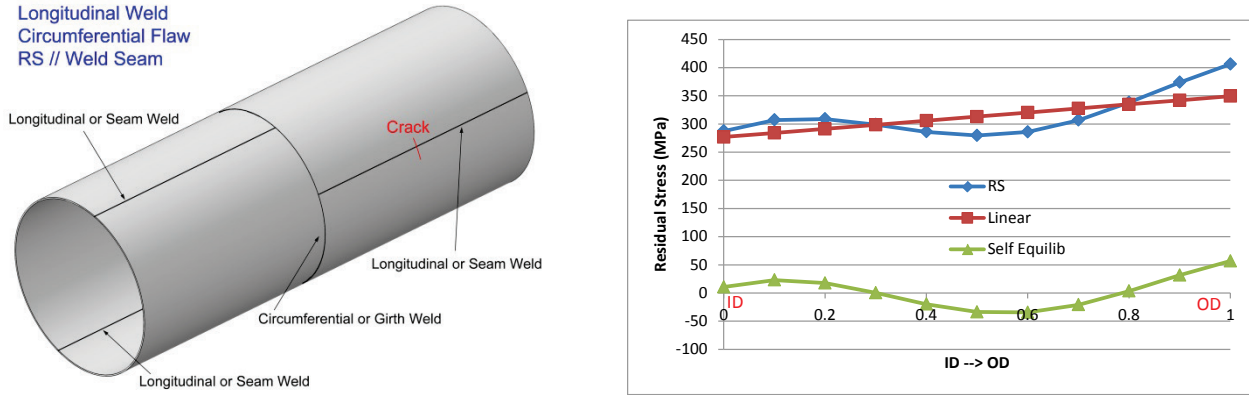


Figure 5 Case 4: Circumferential Crack Perpendicular to an Axial Weld - Residual Stress Parallel to the Axial Weld with a Double-V Notch

Table 2 Coefficients of The Fourth Order Polynomial for Though-Thickness Residual Stress Distribution (σ^R)

$\sigma^R = \sigma_0 + \sigma_1 \left(\frac{x'}{t} \right) + \sigma_2 \left(\frac{x'}{t} \right)^2 + \sigma_3 \left(\frac{x'}{t} \right)^3 + \sigma_4 (x')^4$ <p>($x'=0$ at the outside surface and $x'=t$ at the inside surface)</p>					
Case	σ_0 (MPa)	σ_1 (MPa)	σ_2 (MPa)	σ_3 (MPa)	σ_4 (MPa)
1	314.60	-790.83	-2248.35	7081.99	-4288.01
2	410.99	-190.54	91.54	-339.02	211.26
3	314.13	-800.73	-2323.15	7317.54	-4430.58
4	406.69	-286.26	-683.33	2152.36	-1303.24

Note: t is the wall thickness

FAILURE ASSESSMENT DIAGRAMS (FAD)

The original failure assessment diagram (FAD) [21] is a crack growth resistance curve in terms of the stress or load ratio, L_r (abscissa), and the stress intensity factor or toughness ratio, K_r (ordinate). The stress ratio L_r is defined as the ratio of the applied load (P) to a reference load (P_o), which is the limit load based on net section yielding. To better reflect material behavior under strain hardening, Ainsworth [22] redefined L_r by introducing a reference stress from the primary load as $\sigma_{ref}^p = (P/P_o)\sigma_{ys}$. Therefore, the abscissa for the FAD becomes (API 579 Part 9, Eq. 9.17 [17])

$$L_r^P = \frac{\sigma_{ref}^p}{\sigma_{ys}} \quad (2)$$

API 579 also suggests a modified form for the ordinate of the FAD (K_r). A plasticity interaction factor, Φ , is introduced as a function of L_r^P (the L_r value defined above for the primary load) and L_r^{SR} (the L_r value based on the secondary load, which in the current case is the residual stress). The details can be found in API 579 Part 9 [17]. The modified form for the ordinate is (API 579 Part 9, Eq. 9.26)

$$K_r = \frac{K_I^P + \Phi K_I^{SR}}{K_{mat}} \quad (3)$$

where K_I^P is the stress intensity factor from the primary load, K_I^{SR} is the stress intensity factor from the secondary load (e.g., residual stress), and K_{mat} is the fracture toughness of the material.

The API 579 FAD methodology [17] recommends several versions of material curve for various levels of assessment. These curves are referred as “FAD failure curve,” or “FAD failure envelope,” or simply “FAD” (in Part 9 of API 579). Any assessment point with coordinates (L_r^P , K_r) below the FAD failure curve, the associated crack is mechanically stable; while at the assessment point above the curve is mechanically unstable at the given load and the crack size. Therefore, this flaw is considered unacceptable. A typical FAD is shown in API 579 Part 9, Fig. 9.20 [17]. For API 579 Level 2 and Level 3 (Method A) Assessments [17], the FAD failure curve is defined by Eq. (4):

$$K_r = [1 - 0.14(L_r^P)^2]\{0.3 + 0.7 \exp[-0.65(L_r^P)^6]\} \quad (4)$$

for $L_r^P \leq L_{r(max)}^P$. In the case of austenitic stainless steels, the maximum permitted value (or cut-off value) of L_r^P is $L_{r(max)}^P = 1.8$.

The values of reference stress σ_{ref}^p and the stress intensity factor K_I^P from the primary load are calculated for the loading conditions given in Table 1 with the formulae provided in API 579 (primarily from Part 9, Annexes C and D) [17] as described in the next section. The values of L_r^{SR} and K_I^{SR} , for the current analysis, are calculated with the residual stress distributions across the thickness of the canister shell where the crack is located (see Figs. 2 to 5 and Table 2).

The yield stress of the material for this analysis is 205 MPa (30 ksi) which is based on the ASME minimum yield strength for 304 stainless steel [15] as discussed earlier. Comprehensive testing program of stainless steel system materials under the Savannah River Reactor Materials Program was completed in the early 1990s. The room temperature and 125 °C data for the tensile, Charpy, and fracture toughness of the base metal, weld metal

and the HAZ along C-L and L-C directions were reported for Type 304 stainless steel large diameter piping joined with Type 308 stainless steel weld filler [20]. The lowest fracture toughness at 125 °C for the HAZ is $K_{JC} = 207 \text{ MPa}\sqrt{\text{m}}$, where K_{JC} is converted from J_{IC} obtained from the J - R curve testing with 0.394T-CT specimens in C-L direction. However, at that temperature only two samples were tested and the data range was large: 175-239 $\text{MPa}\sqrt{\text{m}}$. Therefore, the fracture toughness for the current FAD analysis adopts the recommendation from API 579 Annex F *Materials Properties for a FFS Assessment*, Section 4.8.2 [17], from which the base metal $K_{mat} = 220 \text{ MPa}\sqrt{\text{m}}$ (or 200 $\text{ksi}\sqrt{\text{in}}$) is chosen since the flaws are assumed to be initiated in the HAZ.

Reference Stress and Stress Intensity Factor Solutions

The calculations of the reference stress and the stress intensity factor for four crack configurations depicted in Figs. 2 to 5 are described in subsequent sections. The equations are reproduced from API 579-1/ASME FFS-1, 2007 [17]. Only the main equations are listed here. For consistency, the parameter symbols are adopted exactly as those used in API 579 [17]. Care must be taken because the same symbol may be defined differently for different crack configurations considered in API 579 Annexes C and D, respectively, for stress intensity factor and reference stress [17].

In addition, the equations reported in this paper are selected from API 579 [17] for best use with the loading conditions in Table 1. Therefore, the loadings involve only the internal pressure (p), the deadweight (normal), and the axial handling or acceleration (accident). The net section bending moments (M) and the crack face pressure (p_c) are not considered and therefore they are set to zero. However, it should be noted that the welding residual stress does have a bending component and appropriate equations must be used. As discussed earlier, the residual stress is typically expressed as a fourth order polynomial (e.g., Table 2), or represented by the combination of a membrane and a bending stress (e.g., Eqs. 11 and 12).

(1) Axial Through-Wall Cracks

Reference Stress (σ_{ref})

The following equation (Eq. 5) is provided by API 579 Annex D, Eq. D.46 [17] to calculate the reference stress (σ_{ref}) when the membrane (P_m) and bending (P_b) stresses are given:

$$\sigma_{ref} = \frac{P_b + [P_b^2 + 9(M_t P_m)^2]^{0.5}}{3} \quad (5)$$

where M_i is a surface correction factor (API 579 Annex D, Eq. D.8 [17]), which is a function of shell factor $\lambda = \frac{1.818c}{\sqrt{R_i t}}$, R_i is inside radius of the cylinder, and c is the half crack length.

For a general stress distribution through the wall thickness at the location of the crack, the stress ($P(x)$) can be expressed by a fourth order polynomial (see Table 2 and API 579 Annex D, Eq. D.3 [17]):

$$P(x) = P_0 + P_1 \left(\frac{x}{t}\right) + P_2 \left(\frac{x}{t}\right)^2 + P_3 \left(\frac{x}{t}\right)^3 + P_4 \left(\frac{x}{t}\right)^4 \quad (6)$$

and the membrane (P_m) and bending (P_b) components are expressed as

$$P_m = P_0 + \frac{P_1}{2} + \frac{P_2}{3} + \frac{P_3}{4} + \frac{P_4}{5} \quad (7)$$

$$P_b = -\frac{P_1}{2} - \frac{P_2}{2} - \frac{9P_3}{20} - \frac{6P_4}{15} \quad (8)$$

For the canister considered in this study, the axial stress applied to the cylinder does not contribute to the reference stress or the stress intensity factor in the case of an axial through-wall crack. Only the internal pressure loading (p) is relevant (API 579 Annex D, Eqs. D.47 and D.48 [17]):

$$P_m = \frac{pR_i}{t} \quad (9)$$

$$P_b = \frac{pR_o^2}{R_o^2 - R_i^2} \left[\frac{t}{R_i} - \frac{3}{2} \left(\frac{t}{R_i}\right)^2 + \frac{9}{5} \left(\frac{t}{R_i}\right)^3 \right] \quad (10)$$

where R_o is the outside radius of the cylinder.

The reference stress is also calculated for the secondary stress, which in the present case is the welding residual stress. As previously discussed, the residual stress can be curve fitted into a fourth order polynomial (see Table 2 or Eqs. 6-8, where σ_i and P_i are interchangeable, $i= 0$ to 4). However, sometimes it is more convenient to use the direct forms of membrane (P_m) and bending (P_b) stresses, in analog to Eq. (1):

$$P_m = \bar{\sigma}_m^r \sigma_{ys}^r R_r \quad (11)$$

$$P_b = \bar{\sigma}_b^r \sigma_{ys}^r R_r \quad (12)$$

where $\bar{\sigma}_m^r$ and $\bar{\sigma}_b^r$ have already been obtained in the estimation for residual stress (see the paragraph above Eq. 1).

Stress Intensity Factor (K_I)

The stress intensity factor based on API 579 Annex C, Eq. C.156 [17] is

$$K_I = [(\sigma_m + p_c)G_0 + \sigma_b (G_0 - 2G_1)]\sqrt{\pi c} \quad (13)$$

where p_c is the crack face pressure (if any), σ_m and σ_b are membrane stress and through-wall bending stress components, respectively, G_0 and G_1 are influence coefficients and are functions of λ and t/R_i from API 579 Annex C, Tables C.6 (for through-wall crack tip on inside surface) and C.7 [17] (for through-wall crack tip on outside surface). For pressure loading only, the stress intensity factor can be simplified as (API 579 Annex C, Eq. C.158) [17]

$$K_I = \frac{pR_o}{t} G_p \sqrt{\pi c} \quad (14)$$

where G_p is also calculated from Tables C.6 and C.7 in API 579 Annex C [17].

Similarly, the residual stresses contribution to the stress intensity factor is calculated with Eq. (13) with σ_m and σ_b , calculated from the residual stress analysis using Eqs. (6)-(8) or (11)-(12).

(2) Circumferential Through-Wall Cracks

Reference Stress (σ_{ref})

For this crack configuration, the reference stress is given by API 579 Annex D, Eq. D.49 [17]:

$$\sigma_{ref} = \frac{P_b + \{P_b^2 + 9[(ZP_m(1-\alpha)^2]^2\}^{0.5}}{3(1-\alpha)^2} \quad (15)$$

where P_m and P_b are membrane and bending stresses defined

previously, $Z = [\pi(R_o^2 - R_i^2)]/[(2 - \tau)R_o t(2\psi - \theta)]$, $\tau = t/R_o$, $\psi = \arccos\left(\frac{\sin\theta}{2}\right)$, $\theta = c/R_m$, and $\alpha = \theta/\pi$ (see Eqs. D.50 to D.54 in API 579 Annex D [17]).

For the loading in this study, the applied load is the internal pressure (p) with a net section axial force (F), and there is no externally applied bending moment. From API 579 Annex D, Eqs. D55-D56 [17]:

$$P_m = \frac{pR_i^2}{R_o^2 - R_i^2} + \frac{F}{\pi(R_o^2 - R_i^2)} \quad (16)$$

$$P_b = 0 \quad (17)$$

Note that the residual stress will include a bending component.

Stress Intensity Factor (K_I)

The same formula as Eq. (13) for the axial through-wall crack is used for the circumferential through-wall crack (API 579 Annex C, Eq. C.161 [17]):

$$K_I = [(\sigma_m + p_c)G_0 + \sigma_b (G_0 - 2G_1)]\sqrt{\pi c} \quad (18)$$

However, the influence functions G_0 and G_1 are obtained from Tables C.8 and C.9 in API 579 Annex C [17]. The membrane stress σ_m is identical to P_m (Eq. 16) as in the reference stress calculation, and the bending stress and crack face pressure are $\sigma_b = p_c = 0$ (Eq. 17) for the present load case (see Eqs. C.166-C.167 in API 579 Annex C [17]).

(3) Axial Part-Through-Wall Cracks

Reference Stress (σ_{ref})

The reference stress for an axial part-through-wall (a surface crack) of infinite length loaded with internal pressure is (API 579 Annex D, Eq. D.60)

$$\sigma_{ref} = \frac{P_b + \{P_b^2 + 9[M_s P_m (1 - \alpha)^2]^2\}^{0.5}}{3(1 - \alpha)^2} \quad (19)$$

where P_m and P_b are calculated from Eqs. (9) and (10), respectively (as noted by API 579 Annex D, Section 5.4.2b [17]), $M_s = 1.0/(1.0 - \alpha)$, $\alpha = a/t$, and a is the depth of this surface flaw. When the through-wall stress distribution at the crack location is represented by a fourth-order polynomial, such as in the case of residual stress, Eq. (19) is still used to evaluate the reference stress, but P_m and P_b will be calculated according to Eqs. (6)-(8) or

(11)-(12). Note that for an outside surface crack, as presumably caused by chloride induced stress corrosion, the x -coordinate in Eq. (6) should be set such that $x=0$ is at the outside surface of the canister as noted in Table 2.

Stress Intensity Factor (K_I)

The stress intensity factor for an outside surface crack in the axial direction due to internal pressure p is calculated as (API 579 Annex C, Eq. C.176 [17])

$$K_I = \frac{pR_i^2}{R_o^2 - R_i^2} \left[2G_0 + 2G_1 \left(\frac{a}{R_o} \right) + 3G_2 \left(\frac{a}{R_o} \right)^2 + 4G_3 \left(\frac{a}{R_o} \right)^3 + 5G_4 \left(\frac{a}{R_o} \right)^4 \right] \sqrt{\pi a} \quad (20)$$

The influence functions, G_0 , G_1 , G_2 , G_3 , and G_4 , are evaluated according to Table C.10 in Annex C of API 579 [17]. Note that the validity range of these formulae is $0 \leq a/t \leq 0.8$ and $0 \leq t/R_i \leq 1$.

When the stress distribution is expressed as a fourth order polynomial, the Eq. C.177 in API 579 Annex C [17] is used to calculate the stress intensity factor:

$$K_I = \left[G_0(\sigma_0 + p_c) + G_1\sigma_1 \left(\frac{a}{t} \right) + G_2\sigma_2 \left(\frac{a}{t} \right)^2 + G_3\sigma_3 \left(\frac{a}{t} \right)^3 + G_4\sigma_4 \left(\frac{a}{t} \right)^4 \right] \sqrt{\pi a} \quad (21)$$

The coefficients of the fourth order polynomial (σ_i , $i=0$ to 4) are defined identically to Eq. (6) (by replacing P_i by σ_i), and the influence coefficients (G_i , $i=0$ to 4) are functions of t/R_i and a/t , and are obtained from Table C.10 in API 579 Annex C [17]. In the case of residual stress for this canister, the coefficients in Table 2 are used to calculate Eq. (21).

(4) 360° Circumferential Part-Through-Wall Cracks

Reference Stress (σ_{ref})

Using API 579 Annex D, Eq. D.63 [17], the reference stress for a 360° circumferential part-through-wall crack with depth a on the outside surface of the cylinder is

$$\sigma_{ref} = \frac{M_r}{2} + \left(N_r^2 + \frac{M_r^2}{4} \right)^{0.5} \quad (22)$$

The expressions for N_r and M_r depend on the location of the surface crack. For an outside surface crack, Eqs. D.66 and D.67 in API 579 Annex D are used:

$$N_r = \frac{P_m(R_o^2 - R_i^2)}{(R_o - a)^2 - R_i^2}$$

and

$$M_r = P_{bg} \frac{3\pi}{16} \frac{(R_o^4 - R_i^4)}{R_o(R_o - a)^3 - R_i^4}$$

where the membrane stress P_m is calculated exactly as Eq. (16), that is, $P_m = \frac{pR_i^2}{R_o^2 - R_i^2} + \frac{F}{\pi(R_o^2 - R_i^2)}$, and M_r is proportional to the resultant net section bending moment (M) through parameter P_{bg} (API 579 Annex D, Eq. D.69) and is expressed as $P_{bg} = (MR_o)/[0.25\pi(R_o^4 - R_i^4)]$. In the absence of bending moment, Eq. (22) is reduced to

$$\sigma_{ref} = N_r = \frac{P_m(R_o^2 - R_i^2)}{(R_o - a)^2 - R_i^2} \quad (23)$$

When a fourth order polynomial is used to represent the through-thickness stress distribution at the crack location, the following equation is suggested by API 579 Appendix D Eqs. D.70 to D.73 [17]:

$$\sigma_{ref} = \frac{P_b + [P_b^2 + 9(ZP_m(1 - \alpha)^2)^2]^{0.5}}{3(1 - \alpha)^2} \quad (24)$$

where $Z = [1 - \alpha(2 - 2\tau + \alpha\tau/(2 - \tau))]^{-1}$, $\tau = t/R_o$, and $\alpha = a/t$.

Stress Intensity Factor (K_I)

The stress intensity factor for a 360° circumferential part-through-wall (surface) crack under internal pressure (p), crack face pressure (p_c), net section bending moment (M), and a net section axial force (F) is given by API 579 Annex C, Eq. C.178 [17]:

$$K_I = \left[G_0(\sigma_0 + p_c) + G_1\sigma_1 \left(\frac{a}{t} \right) \right] \sqrt{\pi a} \quad (25)$$

For an outside surface crack, according to API 579 Annex C, Eqs. C.181 to C.184 [17], the coefficients σ_0 and σ_1 are given by $\sigma_0 = \sigma_m + \sigma_b$, $\sigma_1 = -2\sigma_b$, and the membrane and bending stresses are

$$\sigma_m = \frac{pR_i^2}{R_o^2 - R_i^2} + \frac{F}{\pi(R_o^2 - R_i^2)} + \frac{2M(R_o + R_i)}{\pi(R_o^4 - R_i^4)} \quad (26)$$

$$\sigma_b = \frac{2M(R_o - R_i)}{\pi(R_o^4 - R_i^4)} \quad (27)$$

For present loading, $M = p_c = 0$. The influence functions G_0 and G_I are provided by Table C.11 in API 579 Annex C [17].

Alternatively, the stress intensity factor can be calculated with a fourth order polynomial stress distribution such as in the case of residual stress. From API 579 Annex C, Eq. C.185 [17]

$$K_I = \left[G_0(\sigma_0 + p_c) + G_1\sigma_1 \left(\frac{a}{t}\right) + G_2\sigma_2 \left(\frac{a}{t}\right)^2 + G_3\sigma_3 \left(\frac{a}{t}\right)^3 + G_4\sigma_4 \left(\frac{a}{t}\right)^4 \right] \sqrt{\pi a} \quad (28)$$

The coefficients of the fourth order polynomial (i.e., σ_i , $i=0$ to 4) are defined similarly as in Eq. (6). The influence functions, G_i ($i=0$ to 4), are provided in Table C.11 of API 579 Annex C [17]. Note that Eq. (28) has the same form as Eq. (21), only the parameters G_i are obtained from different API-provided Tables.

DETERMINATION OF CRACK STABILITY

Only bounding flaw configurations are considered in the present work for evaluating flaw stability for the MPC. These flaw configurations are: axial through-wall crack, circumferential through-wall crack, axial part-through-wall crack, and 360° circumferential part-through-wall crack. These cracks are all assumed to initiate in the HAZ near the axial (seam) weld or the circumferential (girth) weld. Each of the flaw configuration and its relative location with respect to the neighboring welds are illustrated in Figures 2 to 5. The instability crack sizes (depth or length) are calculated with the given loading conditions in Table 1 corresponding to a typical spent nuclear fuel multipurpose canister (HI-STORM) [13,18,19].

Crack Assessment Locus

For a given crack size (i.e., the crack length of a through-wall flaw or the crack depth for a part-through-wall flaw) and a set of external loads and welding residual stress, the coordinates (L_r^P , K_r) for crack instability evaluation with FAD can be calculated based on the reference stress and the stress intensity factor solutions discussed in previous sections. This section describes the construction of a crack assessment locus by gradually

increasing the crack size under the same loading condition. As depicted by Fig. 6, a FAD failure curve defined by Eq. 4 is first plotted. Any assessment point (L_r^P, K_r) below this curve is safe and above is unsafe. In this section the most limiting crack configuration is used for demonstration, that is, an axial through-wall crack with length $2c$. When the residual stress is not considered or it has been relieved by post-weld heat treatment, a “sampling” crack with length 100 mm subject to normal operating loads (Table 1) is stable, as shown by the locus in Fig. 6 labeled as “Normal No RS.” When the crack length is gradually increased, the assessment locus eventually intersects the FAD failure curve (Eq. 4) at $2c = 690$ mm. At this point the critical crack length is defined as 690 mm, beyond which the crack will become unstable under normal operation condition. Similarly, when the residual stress in the direction parallel to the circumferential weld is included (to open the axial crack – see the inset in Fig. 6) and the canister is under normal operating condition, the instability crack length is estimated to be 118 mm by the assessment locus labeled as “Normal with RS.” Under the accident loading condition and with the presence of residual stress (locus labeled as “Accident with RS”), the instability crack length is reduced to 88 mm. These instability crack lengths are reported as part of Table 3 for the axial through-wall flaws.

It is interesting to note that, for this axial through-wall crack, the failure mode of “Normal with RS” appears to be within the range of “Zone 1 Fracture (Elastic) Controlled” as illustrated by Fig. D.1 (FAD) in API 579 Annex D [17]. The failure mode for the locus “Accident with RS” is moving away from the K -dominant elastic regime and it appears to be a borderline Zone 2 Fracture (Elastic-Plastic) and Collapse Controlled.” Furthermore, when the residual stress is not considered and the normal operating load is applied (“Normal No RS”), the failure mode is unmistakably elastic-plastic controlled, which is typical for austenitic stainless steel structures. Note that the boundaries between these zones shown in Fig. D.1 [17] is somewhat arbitrary. Nevertheless, this demonstration has shown that the residual stress will have profound influence on the instability crack length as well as the failure mode (brittle or ductile). For the canister loading given in Table 1, none of the four flaw configurations (Figs. 2 to 5) show totally collapse controlled failure (Zone 3 in Fig. D.1 in API 579 Annex D [17]), which is within the triangular region on FAD defined by $(L_r^P, K_r) = (0,0)$, $(L_{r(max)}, 0)$, and $(L_{r(max)}, K_r|_{L_r^P=L_{r(max)}})$, where $L_r^P = L_{r(max)}$ is the cut-off value (1.8 for stainless steel), and $K_r|_{L_r^P=L_{r(max)}}$ is the K_r value corresponding to $L_r^P = L_{r(max)}$ on the failure assessment curve (Eq. 4). Note that $L_{r(max)}$ is identical to $L_{r(max)}^P$, the symbol that is mostly used in API 579 [17] and in this paper.

It is highlighted that the API FAD approach and assumptions used in this present analysis to estimate instability crack sizes in canisters with welding residual stress is very conservative. It is assumed that the constant residual stress distribution acts on the crack over its entire length or depth, regardless of how long or how deep the crack is, even for the case where the crack has already extended beyond the region dominated by the residual stress. This stress distribution contributes to the value of K_I^{SR} , which is then added to K_I^P (due to the

primary loads such as those in Table 1) through a plasticity interaction factor Φ to give the total value of K_r (see Eq. 3). As a result, K_r increases rapidly with crack size. The conservatism is exacerbated if the through-wall residual stress distribution is overly estimated. In the present analysis, the residual stress is obtained by using API 579 Annex E procedure [17] through a conservative assumption for the heat input density parameter \hat{Q} .

With the residual stress loading the crack, K_r (the ordinate of the FAD) rises rapidly with crack size and eventually intersects the FAD failure curve defined by Eq. 4, as shown in Figure 6. That is, the instability condition is met quickly whereas there is only by a small change of L_r^P as the crack increases in size. This rapidly increasing K_r , having a steep slope with respect to L_r^P , is also responsible for pushing the assessment locus to the Zone 1 regime in the FAD. This is an artifact due to the application of the API procedure because stainless steels are well known as ductile and tough materials. The true assessment points for a stainless steel with an increase in flaw size should most likely traverse within the Zone 2 or Zone 3 in the FAD, as demonstrated in Figure 6 by the assessment locus without residual stress. This finding illustrates the need for a realistic determination of residual stress, and perhaps to employ API Level 3 Method E Assessment (by analysis) [17].

Also note that the instability flaw size would depend on K_{mat} , which in the present analysis is a constant value ($220 \text{ MPa}\sqrt{\text{m}}$ or $200 \text{ ksi}\sqrt{\text{in}}$). If the API 579 Level 3 Method D (Part 9 [17]) were adopted, then the *equivalent* material toughness at each assessment point would be converted from the test data on the J - R curve as recommended by API 579 Annex F [17]. Because the J - R curve can typically be expressed by a power law in terms of crack size increment, the K_{mat} in Eq. (3) is no longer a constant, but is a monotonically increasing function of crack size but with a decreasing slope. By that API procedure (Level 3 Method D), the resulting assessment locus would exhibit a “fish hook” shape as shown in API 579 Part 9, Figure 9.21 [17], where the K_r first decreases to a minimum value and then increases. The instability crack size in this case is then defined when the assessment curve is tangent to the FAD failure curve, or Eq. (4). The reliable J - R curves for this material, especially in the HAZ, are not available at this time. Therefore, this option is not exercised in the present work.

The approach for the determination of instability crack length or depth in this paper is similar to that developed for the high level radioactive nuclear waste tanks at the U. S. DOE Savannah River Site (SRS) by Lam [23] and by Lam and Sindelar [24], in which various FAD methodologies were discussed.

Instability Crack Size

The flaw size obtained at the intersection point of the assessment locus and the FAD failure curve (Eq. 4) as discussed in previous section is defined as the instability crack length or depth for a crack under a given load with or without welding residual stress. The results are summarized in Tables 3 to 6. The flaw tolerance determined previously by Chu [13] using limit load or net section yielding approach is also included for comparison purpose. A significant reduction in the instability crack size can be seen by the inclusion of welding residual stress in the analysis with the framework of FAD, which covers the full range of material deformation modes from purely elastic to elastic-plastic and finally the perfectly plastic collapse failure.

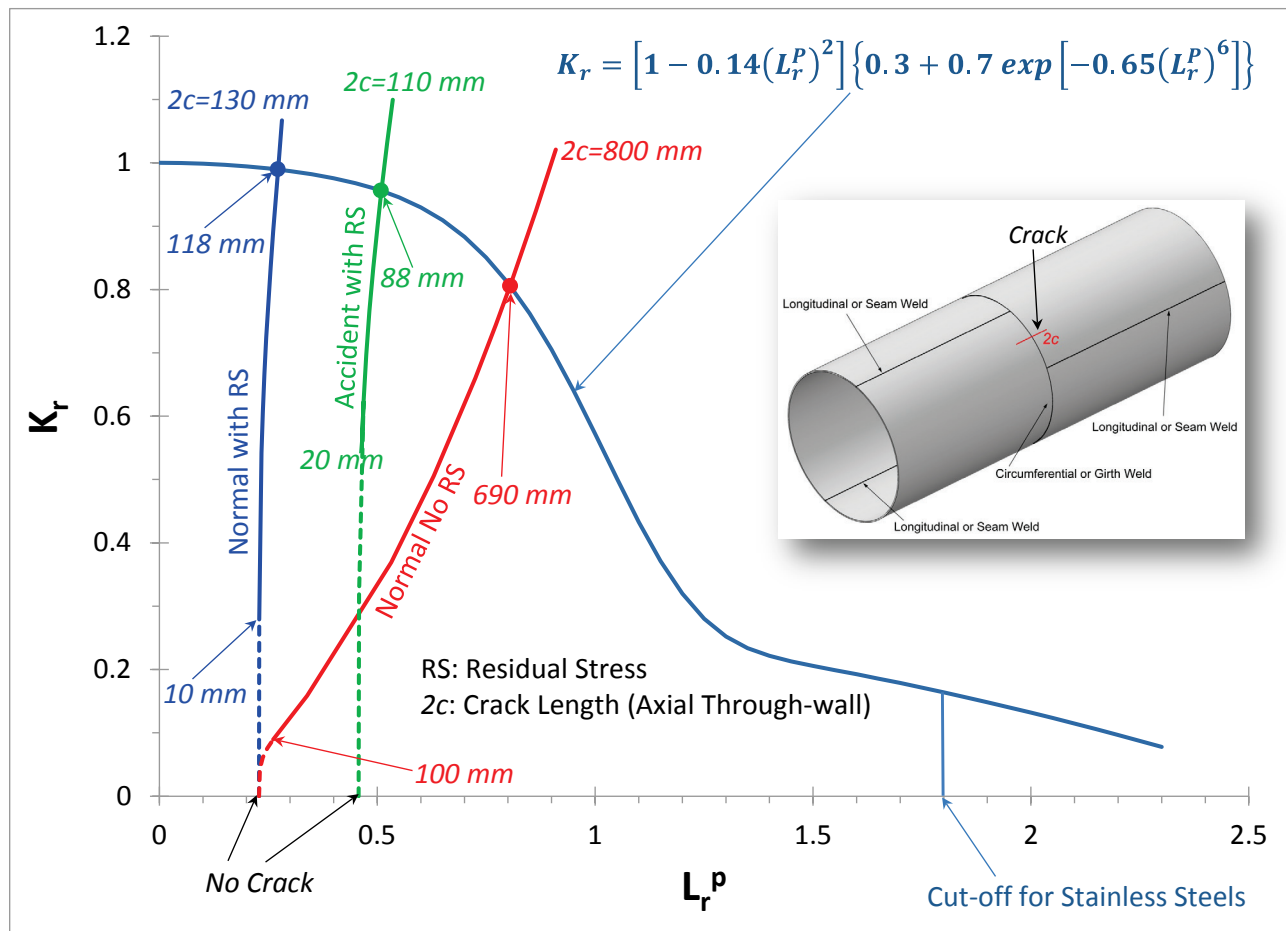
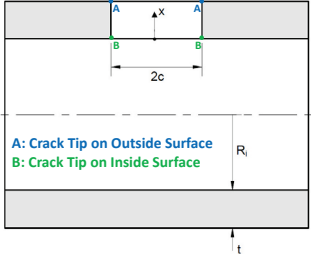
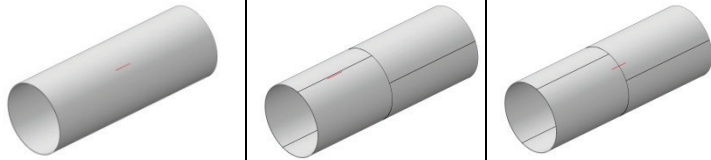


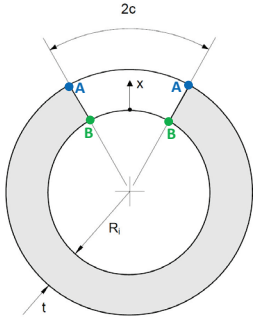
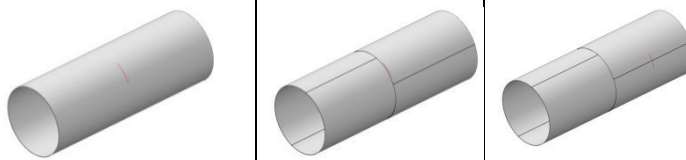
Figure 6 Failure Assessment Diagram and Crack Assessment Loci to Determine Instability Crack Length For an Axial Through-Wall Flaw

Table 3 Instability Crack Length (2c): Axial Through-Wall Crack (Units: mm)

	EPRI [13] (based on Limit Load)	FAD (No Residual Stress)	FAD (Axial Crack // Axial Weld)	FAD (Axial Crack \perp Circumferential Weld)	Crack Tip Location
Normal	1200	730 (outside)	334* (outside)	128 (outside)	 <p>A: Crack Tip on Outside Surface B: Crack Tip on Inside Surface</p>
		690* (inside)	338 (inside)	118* (inside)	
Accident	600	334* (outside)	226* (outside)	102 (outside)	
		350 (inside)	234 (inside)	88* (inside)	
Crack Configuration					

Note: An asterisk “*” denotes the limiting instability crack length for each of the crack-weld configuration.

Table 4 Instability Crack Length (2c): Circumferential Through-Wall Crack (Units: mm)

	EPRI [13] (based on Limit Load)	FAD (No Residual Stress)	FAD (Circumf. Crack // Circumf. Weld)	FAD (Circumf. Crack \perp Axial Weld)	Crack Tip Location
Normal	3300	1543 (outside)	614 (outside)	160* (outside)	 <p>A: Crack Tip on Outside Surface B: Crack Tip on Inside Surface</p>
		1124* (inside)	554* (inside)	180 (inside)	
Accident	2800	1079 (outside)	255 (outside)	141* (outside)	
		860* (inside)	241* (inside)	156 (inside)	
Crack Configuration					

Note: An asterisk “*” denotes the limiting instability crack length for each of the crack-weld configuration.

Table 5 Instability Crack Depth (a/t): Long Axial Part-Through-Wall Crack

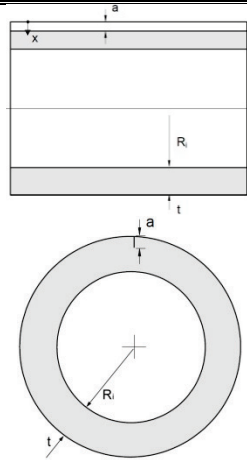
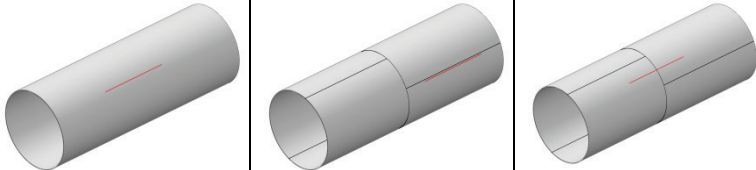
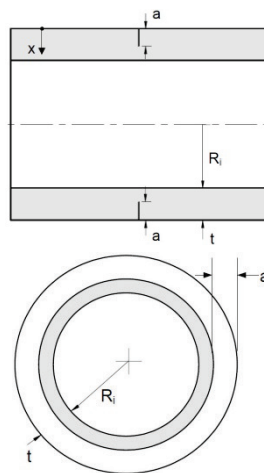
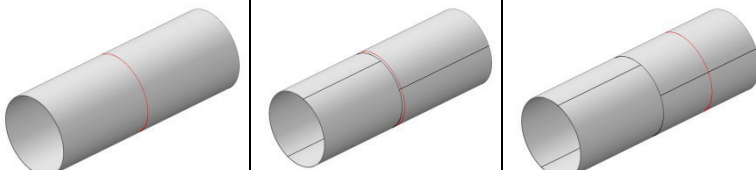
	EPRI [13] (based on Limit Load)	FAD (No Residual Stress)	FAD (Axial Crack // Axial Weld)	FAD (Axial Crack \perp Circumferential Weld)	Cracked Cross-section
Normal	86%	80%	70%	51%	
Accident	73%	63%	57%	43%	
Crack Configuration					

Table 6 Instability Crack Depth (a/t): 360° Circumferential Part-Through-Wall Crack

	EPRI [13] (based on Limit Load)	FAD (No Residual Stress)	FAD (Circumf. Crack // Circumf. Weld)	FAD (Circumf. Crack \perp Axial Weld)	Cracked Cross- section
Normal	91%	92%	>80% (Exceed limit for valid elastic solution)	61%	
Accident	84%	83%	76%	56%	
Crack Configuration					

FLAW ACCEPTANCE LOGIC

The flowchart in Figure 7 represents a general approach for the flaw disposition. It should be noted that, when the depth (a) of a part-through-wall crack exceeds certain fraction of the shell thickness (t), the crack should be recategorized as a through-wall crack due to the uncertainties in sizing, and the high stress intensity at the crack tip leading to uncertainties in the elastic fracture mechanics evaluation to justify stability. When this occurs, the requirement for the through-wall instability for a crack with length ($2c$) must be met. This limit of applicability for the part-through-wall crack is tentatively set to $a/t = 0.8$, beyond which the elastic solution for the stress intensity factor becomes invalid. The frequency of inservice inspection will depend on the amount of subcritical crack growth (or crack growth rate), but it is outside the scope of the present work.

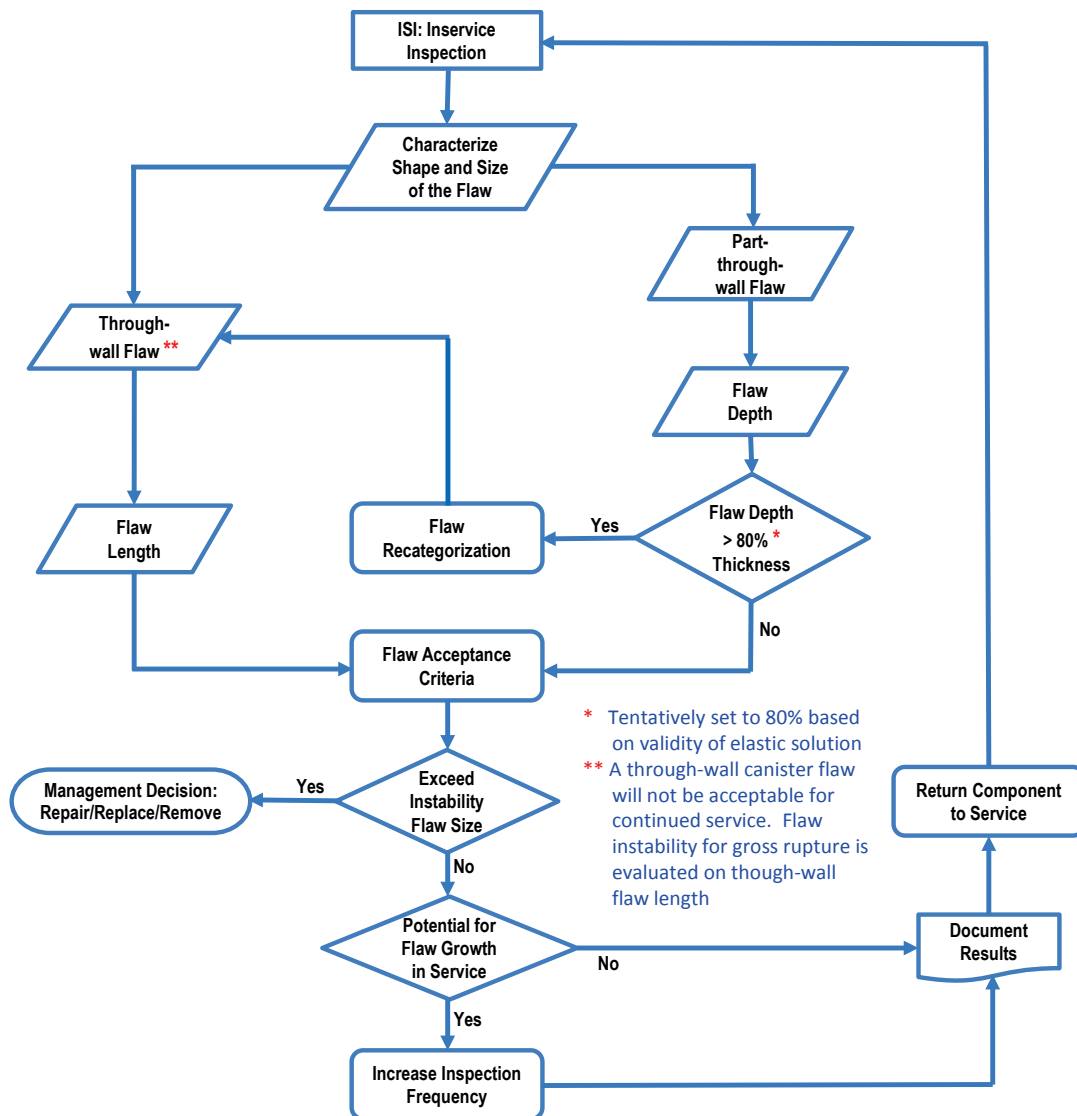


Figure 7 Flaw Acceptance Logic Proposed for a Multi-Purpose Canister

SUMMARY AND PATH FORWARD

Tables 3 to 6 summarize the instability crack sizes developed in the current work with the failure assessment diagram approach. The results show significant effects from the welding residual stress, as well as the orientation of the crack with respect to the weld (and consequently to the direction of the residual stress). It was found that the most limiting lengths for a through-wall axial crack are 118 mm (under normal operating condition) and 88 mm (under accident or off-normal condition), and these constitute only about 10% of the crack lengths proposed earlier through a limit load approach without considering welding residual stresses [13]. Similarly, for a through-wall circumferential crack, the most limiting lengths are 160 mm (normal) and 141 mm (accident), and are about 5% of the earlier reported values. These circumferential crack lengths correspond to very small crack angles about 10° . These new estimates of the instability crack lengths based on FAD severely limit the flaw tolerance when the flaw penetrates the shell thickness and becomes through-wall. For part-through-wall flaws, the severity may be less impacted. The most limiting crack depths for a very long axial part-through-wall crack are 51% and 43% of the shell thickness, respectively, for normal and accident conditions. These crack depths are about 60% of the previously proposed values. In the case of a circumferential part-through-wall crack that circumvents around the entire canister (360°), the most limiting crack depths are 61% (normal) and 56% (accident) of the shell thickness. They are about 70% of the values based on net section yielding without residual stress.

For a more accurate flaw stability analysis, a semi-elliptic crack configuration should be considered to calculate the instability crack depth for a surface crack. Since additional parameters are needed to define the crack front (crack length and crack depth), the calculation based on API 579-1/ASME FFS-1 [17] becomes much more complicated, but is still feasible. It is expected that the flaw stability criteria based on the semi-elliptic cracks with a FAD approach would be less limiting (i.e. would show larger stable crack sizes) than the ones developed here with extreme bounding configurations (e.g., an infinitely long axial surface crack and a full- 360° circumferential surface crack).

It has been shown that the welding residual stress acting on crack significantly affects the instability crack size, and welding residual stresses should be included in the analysis as a secondary load (stress). This leads to a conclusion that a more accurate welding residual stress should be used in developing the flaw disposition acceptance criteria. Therefore, more information on the weld geometry (such as single- or double-V notches) and the actual welding parameters (such as the electric current, voltage, electrode travel speed, and the number of passes) used in canister fabrication would enable a more accurate estimation of residual stress. Finally, the loadings must be clearly defined for various types of canisters, and the canister-specific flaw stability criteria could be developed.

A comprehensive approach for the determination of accurate flaw stability with residual stress should consider a full set of numerical analyses that includes welding simulation and fracture mechanics analysis (such as Lam et al. [25]). In addition, the residual stress redistribution at crack initiation and subsequence growth will have various degrees of influence on the J-integral based fracture criterion, depending on the relative magnitudes of the residual stress and the applied stress, as recently shown by Zhu [26]. These analytical approaches are categorized under API 579-1/ASME FFS-1 Level 3 Method E Assessment [17]. The comparison of instability crack lengths resulting from various assessment procedures has been carried out for the SRS high level nuclear waste tanks [23,24].

ACKNOWLEDGEMENT

This work at the Savannah River National Laboratory was sponsored by the Nuclear Fuel Storage and Transportation (NFST) Planning Project under the U.S. Department of Energy, Office of Nuclear Energy; and by the Savannah River Nuclear Solutions, LLC under Contract No. DE-AC09-08SR22470 with the U. S. Department of Energy.

REFERENCES

- [1] U. S. NRC, 2014, *Continued Storage of Spent Nuclear Fuel*, Federal Registry, Vol. 79, No. 182/Friday September 19, 2014/Rules and Regulations, United States Government, Washington, DC., USA.
- [2] Kosaki, A., 2005, "The corrosion behavior of one-fifth scale lid models of transport cask submerged in sea bottom," *Corrosion Science*, 47, pp. 2361–2376.
- [3] Kosaki, A., 2006, "SCC Propagation Rate of Type 304, 304L Steels under Oceanic Air Environment," Paper No. ICONE14-89271, Vol. 1, Plant Operations, Maintenance and Life Cycle; Component Reliability and Materials Issues; Codes, Standards, Licensing and Regulatory Issues; Fuel Cycle and High Level Waste Management, International Conference on Nuclear Engineering, July 17-20, Miami, Florida, USA, pp. 443-450
- [4] J. Tani, Mayuzumi, M., Arai, T., and Hara, N., 2007, "Stress Corrosion Cracking Growth Rates of Candidate Canister Materials for Spent Nuclear Fuel Storage in Chloride-Containing Atmosphere," *Materials Transactions*, Vol. 48, No. 6, pp. 1431 to 1437.
- [5] Kosaki, A., 2008, "Evaluation method of corrosion lifetime of conventional stainless steel canister under oceanic air environment," *Nuclear Engineering and Design*, 238, pp. 1233–1240.
- [6] Tani, J., Mayuzumi, M., and Hara, N., 2008, "Stress corrosion cracking of stainless-steel canister for concrete cask storage of spent fuel," *Journal of Nuclear Materials* 379, pp. 42–47.

- [7] Tani, J.I., 2009, "Initiation and Propagation of Stress Corrosion Cracking of Stainless Steel Canister for Concrete Cask Storage of Spent Nuclear Fuel," *Corrosion*, Vol. 65, No. 3, pp. 187-194.
- [8] Caseres, L. and Mintz, T.S., 2010, Atmospheric Stress Corrosion Cracking Susceptibility of Welded and Unwelded 304, 304L, and 316L Austenitic Stainless Steels Commonly Used for Dry Cask Storage Containers Exposed to Marine Environments, NUREG/CR-7030, Office of Nuclear Regulatory Research, U.S. Nuclear Regulatory Commission, Washington, D.C., USA.
- [9] Shirai, K., Tani, J. , and Saegusa, T., 2011, "Study on Interim Storage of Spent Nuclear Fuel by Concrete Cask for Practical Use -Feasibility Study on Prevention of Chloride Induced Stress Corrosion Cracking for Type 304L Stainless Steel Canister," CRIEPI N10035, Central Research Institute of Electric Power Industry , Tokyo, Japan (In Japanese).
- [10] Oberson, G., Dunn, D., Mintz, T., He, X., Pabalan, R., and Miller, L., 2013, "US NRC-Sponsored Research on Stress Corrosion Cracking Susceptibility of Dry Storage Canister," Materials in Marine Environments – 13344, WM2013 Conference, February 24 – 28, 2013, Phoenix, Arizona USA.
- [11] He, X., Mintz, T. S., Pabalan, R., Miller, L., and Oberson, G., 2014, Assessment of Stress Corrosion Cracking Susceptibility for Austenitic Stainless Steels Exposed to Atmospheric Chloride and Non-Chloride Salts, NUREG/CR-7170, Office of Nuclear Regulatory Research, U.S. Nuclear Regulatory Commission, Washington, D.C., USA.
- [12] Chopra, O.K., Diercks, D.R., Fabian, R.R., Han, Z.H. and Liu, Y.Y., 2014, Managing Aging Effects on Dry Cask Storage Systems for Extended Long-Term Storage and Transportation of Used Fuel, Rev. 2," FCRD-UFD-2014-000476, ANL-13/15, U.S. Department of Energy, Washington, D.C., USA.
- [13] Chu, S., 2014, *Flaw Growth and Flaw Tolerance Assessment for Dry Cask Storage Canisters*, No. 3002002785, Electric Power Research Institute, Palo Alto, CA., USA.
- [14] ASME Boiler and Pressure Vessel Code, Section XI, *Rules for Inservice Inspection of Nuclear Power Plant Components*, 2013, American Society of Mechanical Engineers, New York, NY., USA.
- [15] ASME Boiler and Pressure Vessel Code, Section II, Part D, *Properties*, 2011, American Society of Mechanical Engineers, New York, NY., USA.
- [16] Lam, P.S., Sindelar, R.L., Duncan, A.J., and Adams, T.M., 2014, "A Framework to Develop Flaw Acceptance Criteria for Structural Integrity Assessment of Multipurpose Canisters for Extended Storage of Used Nuclear Fuel," Paper No. PVP2014-28990, Proceedings of ASME Pressure Vessels and Piping Conference, Anaheim, California, USA. Also from the U. S. Department of Energy Office of Scientific and Technical Information (OSTI): <http://sti.srs.gov/fulltext/SRNL-STI-2014-00151.pdf>
- [17] API 579-1/ASME FFS-1, 2007, *Fitness-For-Service* (API 579 Second Edition), American Petroleum Institute, Washington, DC., USA.

- [18] Bjorkman, G., Chuang, T.-J., Einziger, R., Malik, S., Malliakos, A., Mitchell, J., Navarro, C., Ryder, R., Shaukat, S., Ulses, A., and Zigh, G., 2007, *A Pilot Probabilistic Risk Assessment of a Dry Cask Storage System at a Nuclear Power Plant*, NUREG-1864, U.S. Nuclear Regulatory Commission Washington, DC., USA.
- [19] <http://www.holtecinternational.com/productsandservices/wasteandfuelmanagement/multi-purpose-canisters/>
- [20] Stoner, K.J., Sindelar, R.L., and Caskey, G.R., 1991, *Reactor Materials Program: Baseline Material Property Handbook — Mechanical Properties of 1950s Vintage Stainless Steel Weldment Components*, WSRC-TR-91-10, Westinghouse Savannah River Company, Aiken, South Carolina, USA. Also from the U. S. Department of Energy Office of Scientific and Technical Information (OSTI): <http://www.osti.gov/scitech/servlets/purl/14751>
- [21] Milne, I, Ainsworth, R.A., Dowling, A.R., and Stewart, A.T., 1986, *Assessment of the Integrity of Structures Containing Defects*, Central Electricity Generating Board Report R/H/R6-Rev. 3, May 1986; Also in International Journal of Pressure Vessel & Piping, Vol. 32, pp. 3-104, 1988.
- [22] Ainsworth, R.A., 1984, “The Assessment of Defects in Structures of Strain Hardening Materials,” Engineering Fracture Mechanics, Vol. 19, pp. 633-642.
- [23] Lam, P.S., 2000, *Comparison of Fracture Methodologies for Flaw Stability Analysis for High Level Waste Storage Tanks*, WSRC-TR-2000-00478, Westinghouse Savannah River Company, Aiken, South Carolina, USA (<http://sti.srs.gov/fulltext/tr2000478/tr2000478.pdf>).
- [24] Lam, P.S., and Sindelar, R.L., 2004, “Comparison of Fracture Methodologies for Flaw Stability Analysis of Storage Tanks,” in *Fracture Methodologies and Manufacturing, Processes*, Proceedings of ASME Pressure Vessels and Piping Conference, San Diego, California, PVP-Vol. 474, pp. 91-103. Also from the U. S. Department of Energy Office of Scientific and Technical Information (OSTI): <http://sti.srs.gov/fulltext/ms2004209/ms2004209.pdf>
- [25] Lam, P.S., Chang, C., Chao, Y.J., Sindelar, R.L., Stefek, T.M., and Elder III, J.B., 2005, “Stress Corrosion Cracking of Carbon Steel Weldments,” PVP2005-71327, Proceedings of ASME Pressure Vessels and Piping Conference, Denver, Colorado. Also from the U. S. Department of Energy Office of Scientific and Technical Information (OSTI): <http://sti.srs.gov/fulltext/ms2005078/ms2005078.pdf>
- [26] Zhu, X.-K., 2015, “Determination of Path-Independent J-Integral for Cracks in Residual Stress Fields Using Finite Element Method,” PVP2015-45712, Proceedings of the ASME Pressure Vessels & Piping Conference, Boston, Massachusetts, July 2015.